Tunable Single-Mode Output by Optical-Mode Selection

Hailang Dai,[1,*,‡] Hong Yang,[1,‡] Zhuangqi Cao,[1] and Xianfeng Chen[1,2,3,†]

[1] *State Key Laboratory of Advanced Optical Communication Systems and Networks, School of Physics and Astronomy, Shanghai Jiao Tong University, Shanghai 200240, China*

[2] *Shanghai Research Center for Quantum Sciences, Shanghai 201315, China*

[3] *Collaborative Innovation Center of Light Manipulations and Applications, Shandong Normal University, Jinan 250358, China*

(Received 21 April 2022; revised 31 October 2022; accepted 6 February 2023; published 14 March 2023)

The ability to manipulate and select optical modes effectively and accurately is strongly desired to enable single-mode operation. Here, we report an optical system consisting of two directly coupled metal-cladded optical resonators that can realize a single-mode peak through control of the tuning between the resonant wavelengths of the two optical resonators. Additionally, the wavelength of the single-mode peak can be chosen via adjusting the angle of incident light. Furthermore, the linewidth and power of the single-mode output can be controlled completely by the thickness of the resonator guide layer and the angle of incident light. This optical system provides a way to realize optical information processing without the need for complex structures and specific materials.

DOI: 10.1103/PhysRevApplied.19.034046

I. INTRODUCTION

Microscale waveguide cavities support large numbers of closely spaced modes because their dimensions are typically much larger than the optical wavelengths [1]. As a result, the stimulated emission outputs from these microscale waveguide cavities are subject to random fluctuations and instabilities caused by mode competition for limited gain. During recent decades, the effective manipulation and accurate selection of modes has been studied intensively to achieve single-mode operation [2,3]. Therein, both spatial and spectral controllability have become requirements to enable enhanced stimulated emission performance with high monochromaticity, reduced mode competition, and perfect beam quality. In traditional manufacture, single-mode operation is achieved based on sufficient modulation of gain and loss [1], but many factors impede wider realization, including inhomogeneous gain saturation [4], excessive mode loss [5], and low effective modulation [6]. Several approaches were developed, including the use of an additional cavity for intracavity feedback [7–9], the use of a distributed feedback grating [10,11], enlargement of the free spectral range through mode-size reduction [12], and the use of spatially varied optical pumping [13]. However, specific design configurations are applied in these approaches. A general design concept that allows flexible control of the cavity modes is still desired. To date, *PT*-symmetric optics [14] offers one way to advance laser science via strategic manipulation of the gain and loss to control light transport. Proposed techniques, such as loss-induced transparency [15], power-oscillation violations [16], *PT*-synthetic photonic lattices [17], and unidirectional invisibility [18], are yet to be realized. Furthermore, a system consisting of two directly coupled microtoroidal whispering-gallery-mode resonators (WGMRs) [19,20] provides direct proof of nonreciprocity in *PT*-symmetric optics, and this has substantial device implications for optical information processing [21]. However, this system mediates the coupling between two directly coupled microtoroidal WGMRs using the thermo-optic effect of silica and different fiber-taper couplers, rather than enabling flexible control of the cavity modes. Recent explorations of metal-cladded optical resonators offer the opportunity to advance laser science by manipulating the angle of incidence strategically to control the wavelength of coupled light [22–25]. Here, we report a system that consists of two directly coupled metal-cladded optical resonators (MCORs) that are able to adjust their angles of incidence using free-space coupling technology. Eventually, by adjusting the angle of incidence, we realize single-mode operation by controlling the difference between the resonator wavelengths of the compound system through resonance-wavelength tuning.

*hailangdai@sjtu.edu.cn

†xfchen@sjtu.edu.cn

‡H. Dai and H. Yong contributed equally to this work.

II. THEORY

A. Structural characterization

As shown in Fig. 1(a), each MCOR consists of three layers: a 0.1-mm-thick BK7 glass layer is used as a guided layer, a 24-nm-thick silver film is used to couple the incident light, and another 300-nm-thick silver film serves as the substrate layer. Compared with conventional all-dielectric optical waveguides, the MCOR offers a variety of fascinating optical properties [22,26–31]. The most unique feature is the presence of ultrahigh-order guided modes (UOMs) [24,32,33] that occur when light illuminates the upper silver film of the MCOR under the coupling condition. The dispersion equation for the mth-order mode of the MCOR can be written as

$$\kappa_1 h_1 = m\pi + 2\arctan\left(\rho\frac{\alpha_2}{\kappa_1}\right), \tag{1}$$

where $\kappa_1 = (k_0^2\varepsilon_1 - \beta^2)^{1/2}$; $\alpha_2 = (\beta^2 - k_0^2\varepsilon_2)^{1/2}$; and ρ has a value of 1 or $\varepsilon_1/\varepsilon_2$ when the incident-light mode is transverse electric (TE) or transverse magnetic (TM), respectively. $k_0 = 2\pi/\lambda_0$ is the propagation constant in a vacuum. n_1 and h_1 are the refractive index and the thickness of the guided layer, respectively. $\beta = k_0 \sin\theta_i$ is the guided-mode propagation constant, θ_i is the angle of incidence, and m is the number of modes. As a result, an

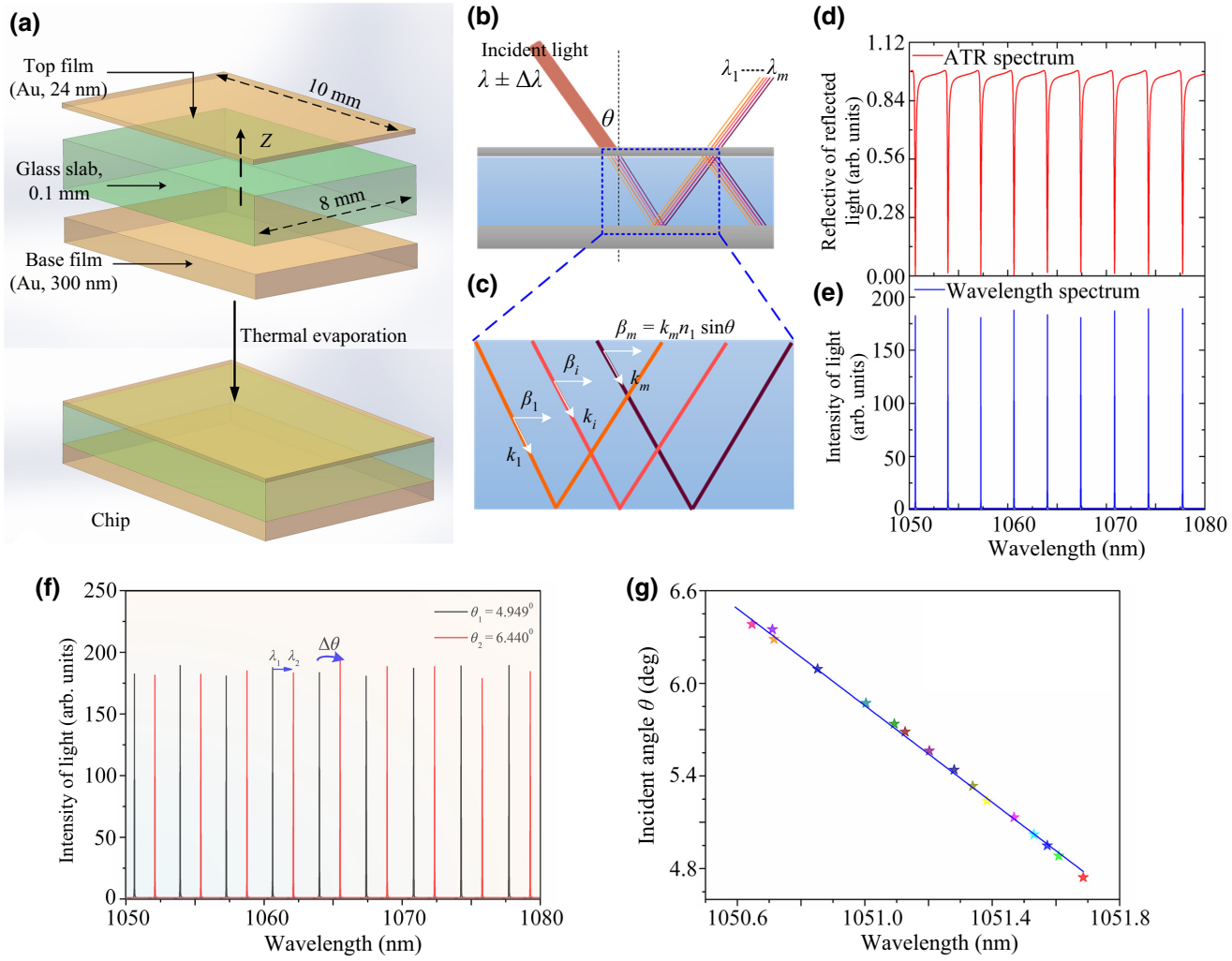

FIG. 1. Metal-cladded optical-resonator structure and associated theory. (a) Fabrication process for a tunable-frequency-matching MCOR. (b) Incident light is coupled into a waveguide layer, and different wavelengths are separated according to scattering theory in an isotropic medium when the linewidth of incident light is $2\Delta\lambda$. (c) Illustration of the relationship between propagation constant β of incident light and wave vector $\hat{k}'$. (d),(e) When the angle of incidence matches the coupling angle, the attenuation of total reflection (ATR) spectrum and an optical-comb spectrum are realized in the reflection direction. (f) When the angle of incidence is changed by $\Delta\theta = \theta_2 - \theta_1$, the optical-comb spectrum shows a redshift of $\delta\lambda$. (g) Using the model eigenvalue equation for the MCOR, we obtain the relationship between shift $\delta\lambda$ and θ.

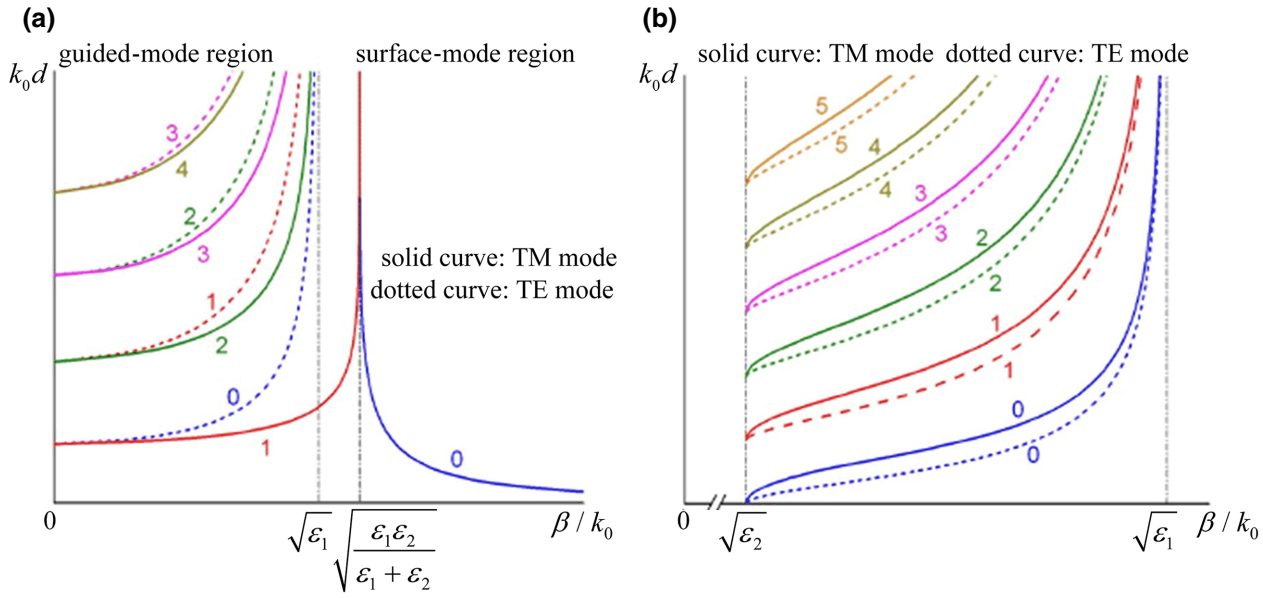

FIG. 2. Dispersion curves of (a) the MCOR and (b) a symmetrical dielectric waveguide.

incident beam that illuminates the MCOR excites standing-wave modes in the guided layer that depend on its angle of incidence and wavelength.

Therein, for a given light frequency, ω, and guiding-layer thickness, d, the propagation constant, β, of the mth TE mode is smaller than that of the mth TM mode. This property of the MCOR is identical to that of the metal-cladded leaky waveguide, but differs from that of a dielectric planar waveguide. The dispersion curves for the MCOR and for a symmetrical dielectric waveguide are shown in Figs. 2(a) and 2(b), respectively. The solid curves represent the TM modes and the dashed curves represent the TE modes. The MCOR is independent of the polarization of incident light. The dispersion curves for the TE and TM modes are qualitatively similar for high-order modes. Therefore, incident light with TE or TM polarization will always suit our waveguide.

B. UOMs

When the guiding-layer thickness reaches the millimeter scale, as Eq. (1) shows, the MCOR can accommodate thousands of guided modes. For example, when using the parameters $\varepsilon_2 = -52.2 + i2.2$ (the metal material is silver), $\varepsilon_1 = 2.278$, $S = 30$ nm, $d = 0.38$ mm, and $\lambda = 1064$ nm, m is 1657 for the highest mode. When the light beam is coupled from free space with a large angle of incidence, it is difficult to differentiate the adjacent guided modes because the mode density in the MCOR is extremely high and the corresponding ATR dips overlap with each other. However, a series of discrete guided modes can be excited at specific extremely small angles of incidence. We term these modes the ultrahigh-order modes [24] because the orders of these modes are extremely large and the effective refractive index of each mode is small. From a ray-optics perspective, within the same longitudinal propagation distance, the UOMs rebound at interfaces more times than the conventional modes, and their ray-propagation lengths are also longer because the angles of incidence of the UOMs at the top and bottom interfaces of the guiding layer are extremely small. Ultimately, the UOMs show better confinement than the conventional modes and their corresponding propagation losses are small, even with the existence of the metal films. Therefore, these modes form standing modes in the guiding layer of the MCOR. Additionally, the UOMs have the slow-light effect, which contributes to their enhanced confinement, and the inner states associated with these modes are standing modes.

C. Wavelength variation relationship with the angle of incident light

According to Eq. (1), we can obtain the relationship between the propagation constant in a vacuum, k_0, and the angle of incidence, θ_i, under TE light polarization conditions:

$$k_0 n_1 \cos\theta_i h_1 = m\pi + 2\arctan\left(\sqrt{\frac{\varepsilon_1 - \varepsilon_2}{\varepsilon_1 \cos^2\theta_i} - 1}\right). \quad (2)$$

When the guiding-layer thickness, h_1, reaches the millimeter scale, the MCOR can accommodate thousands of guided modes, as illustrated in Fig. 1(d) and described by Eq. (1). In addition, a series of discrete guided modes can be excited at certain extremely small angles of incidence because the extremely large mode density in the

MCOR results in the modes overlapping with each other. On the basis of the dispersion equation [Eq. (1)] for the MCOR, we can obtain the approximate formula $\Delta m \propto \sin 2\theta_i \Delta\theta_i$. Because $\Delta m = 1$, when the angle of incidence, θ_i, is smaller, then a larger value of $\Delta\theta_i$ is obtained. This property is convenient for use in the design of an optical comb, as illustrated in Fig. 1(e).

Therein, the angle of incidence is $\theta_i < 5°$, and the value of the second term on the right-hand side of Eq. (1), $\arctan(\alpha_2/\kappa_1)$, is far smaller than m and can be ignored. Therefore, Eq. (2) can be reduced to the following simple equation [34]:

$$\frac{2\pi}{\lambda} n_1 h_1 \cos\theta_i = m\pi, \tag{3}$$

where n_1 and h_1 are the refractive index and the thickness of the guiding slab, respectively. θ_i is the angle of incidence of the light rays inside the waveguide. λ and c are the wavelength and velocity of the light in free space, respectively. Without consideration of the material dispersion of the waveguide, we can express the wavelength spacing between two neighboring channels as $\Delta\nu = c/(2n_1 h_1 \cos\theta_i)$, which becomes a constant when the angle of incidence of the light is fixed. In other words, the channel wavelength spacings for this comb filter are equal. Furthermore, based on Eq. (3), we can see that both the center wavelength and the channel spacing can be tuned by varying the angle of incidence. As shown in Fig. 1(f), when the angles of incidence of the light, θ_i, are 4.949° and 6.440°, we can obtain an optical-comb spectrum. Moreover, switching from an incident wavelength of λ_1 to λ_2 changes the angle of incidence by $\Delta\theta_i = 1.491°$. According to the simple equation above, the angle of incidence, θ_i, and the incident wavelength, λ_i, have a linear relationship, as illustrated by the numerical simulation results shown in Fig. 1(g). Equation (3) can then be reduced to the following:

$$2n_1(1-\theta_i)h_1 = m\lambda_i. \tag{4}$$

According to Eq. (4), the required wavelength variation is achieved by changing the angle of incidence of the laser light. We want to change the wavelength of a single mode by changing the angle of incidence alone. The fundamental analysis results shown in Fig. 1(g) indicate that we can obtain a series of wavelengths by changing the angle of incidence. However, these angles of incidence are discrete because of the mode-order integer.

Moreover, on the basis of the dispersion equation of the MCOR given by Eq. (1), we can obtain the following approximate formula:

$$\Delta m \propto \sin 2\theta_i \Delta\theta_i. \tag{5}$$

Because $\Delta m = 1$, when the angle of incidence, θ_i, is reduced, a larger $\Delta\theta_i$ is obtained as a result. Therefore, the ATR dips for the UOMs are discrete. This property is convenient for use in the design of comb filters for optical-communication applications.

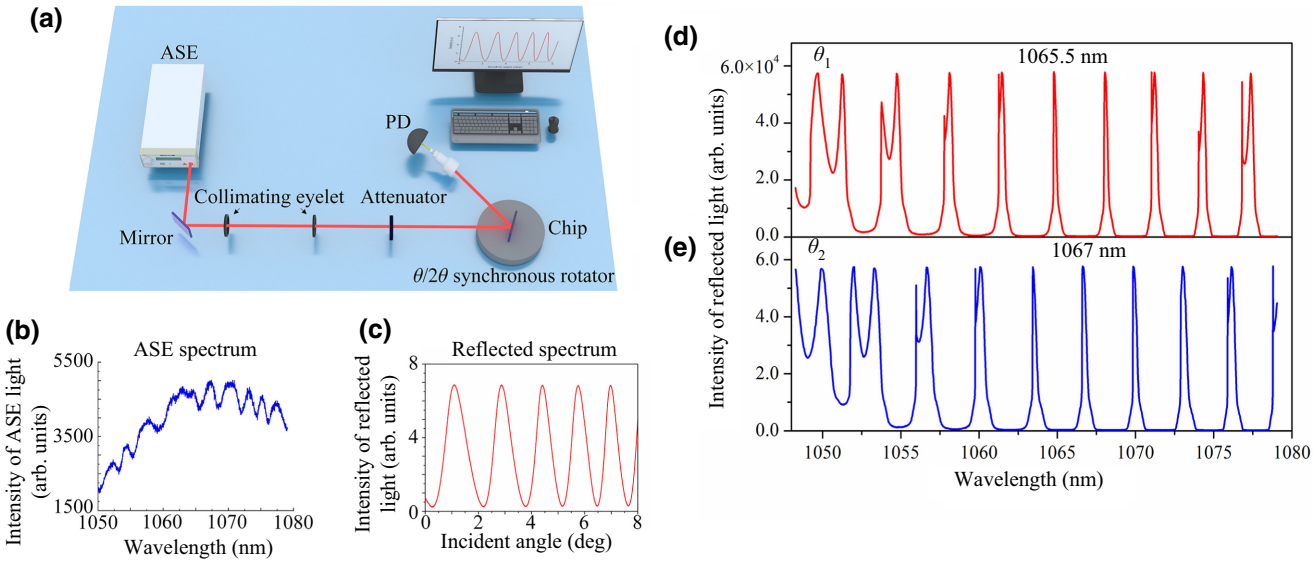

FIG. 3. Differences in separate peaks in the reflected spectrum produced by changing the angle of incidence. (a) Experimental setup. PD, photoelectric detector. (b) ASE source spectrum. (c) Experimental data demonstrating that more than 98% of the power of the 1064-nm-wavelength light is coupled in the chip when incident light reaches the coupling angles. Therein, according to the eigenvalue equation, multiple coupling angles are shown to exist. (d),(e) Continuous-wavelength ASE pumping spectrum is scattered into a series of separate peaks in the reflected spectrum when the pump light is incident on the metal-cladded resonator at different angles of incidence.

III. EXPERIMENT AND RESULTS

Figure 3(a) shows the experimental setup used to produce an optical-comb spectrum. Figure 3(b) shows the amplified spontaneous emission (ASE) source spectrum, which ranges from 1050 to 1080 nm. In the experimental system, the coupling effect of the MCOR is detected, and more than 98% of the incident light is coupled into the MCOR when the angle of incidence reaches the coupling angle, as illustrated in Fig. 3(c). According to Fig. 3(c) and Eq. (1), there are many coupling angles that can be used to reach 98% effective coupling; however, Figs. 3(d) and 3(e) show the optical-comb spectra formed at angles of incidence of $\theta_i = 3.80^\circ$ and 5.15°, respectively. The continuous-wavelength ASE spectrum is scattered into

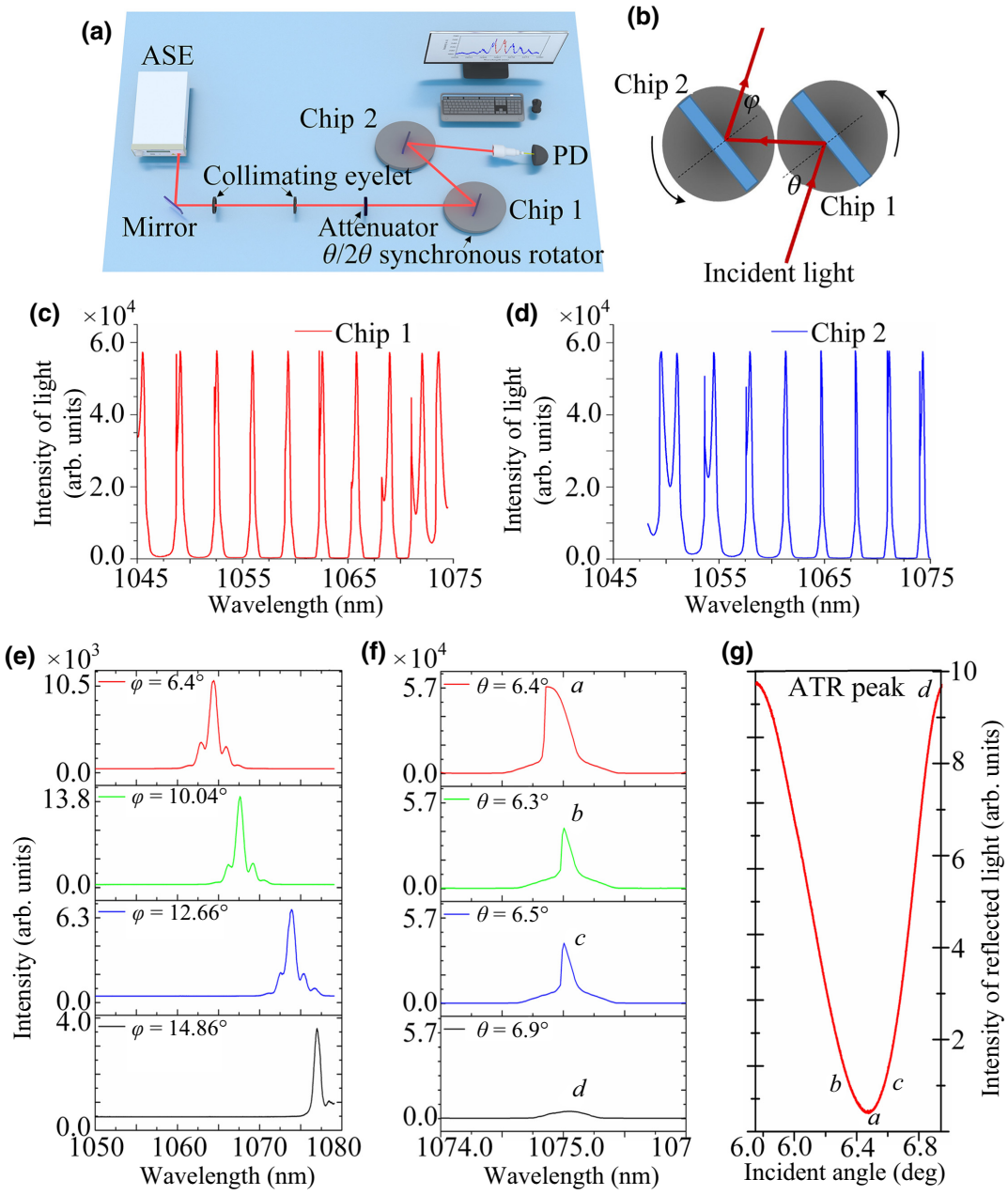

FIG. 4. Wavelength tuning of the metal-cladded optical resonator. (a) Experimental setup. (b) Mode-selection system based on two chips. (c),(d) Optical-comb-spectrum experimental data for chip 1 and chip 2, respectively, at different angles of incidence. Thickness of the waveguide layer in both chip 1 and chip 2 is 0.1 mm, and metal-cladded resonator and substrates are prepared from the same materials under the same conditions. (e) When the angle of incidence, φ, of chip 2 is adjusted and the angle of incidence of chip 1 remains fixed, single-mode spectra shown are obtained from the mode-selection system based on the two chips at angles of incidence of $\varphi_1 = 6.40^\circ$, $\varphi_2 = 10.04^\circ$, $\varphi_3 = 12.66^\circ$, and $\varphi_4 = 14.86^\circ$. (f) When the angle of incidence of chip 2 is $\varphi_3 = 12.66^\circ$, we change the angle of incidence, θ, of chip 1, which results in changes to the intensity of the single mode shown. (g) ATR peak characteristic.

an optical-comb spectrum, and the optical-comb-spectrum wavelengths are different at the angles of incidence of $\theta_i = 3.80°$ and $5.15°$. These experimental data support the theoretical speculation that both the optical-comb wavelength and the channel spacing can be tuned by varying the angle of incidence.

After the theoretical speculation and experimental verification, we design a system that consists of two directly coupled MCORs, as shown in Fig. 4(a), where each MCOR is coupled to enable adjustment of the angle of incidence via free-space-coupling technology. Ultimately, by adjusting the angles of incidence, θ and φ, we

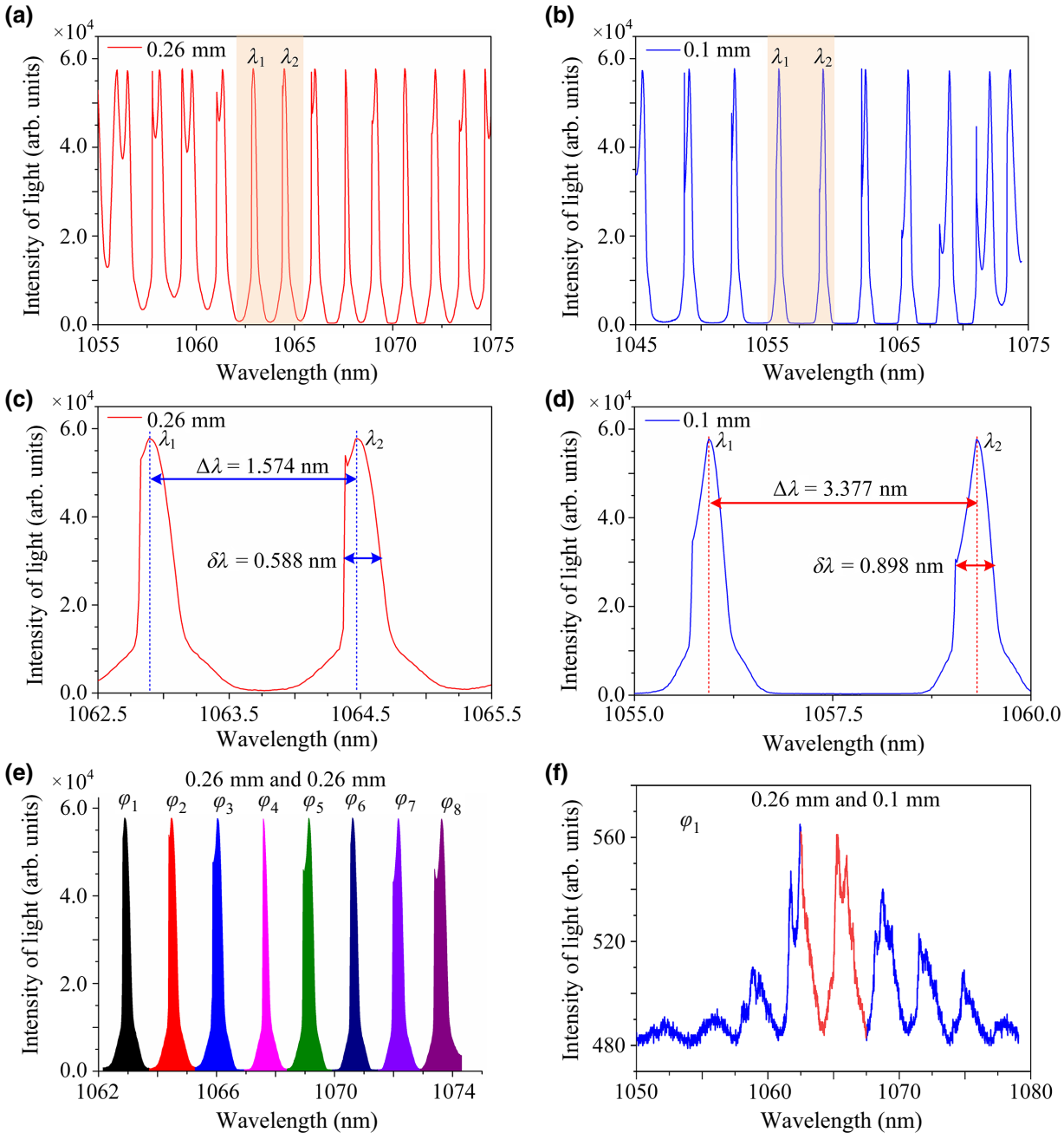

FIG. 5. Characterization of linewidths and continuous-tuning abilities. (a),(b) Experimental optical-comb-spectrum data for waveguide-layer thicknesses of 0.26 and 0.1 mm at the coupling angle, respectively. (c),(d) Linewidths of modes and the distance between modes for 0.26- and 0.1-mm chips, respectively. (e) When the mode-selection system is formed using two 0.26-mm chips, we achieve single-mode output at different angles of incidence, φ, for chip 2. (f) When the mode-selection system is formed using 0.26- and 0.1-mm chips, resonance part is as indicated by the red curve of the spectrum.

produce a single-mode peak by controlling the detuning between the resonant wavelengths of the MCORs through tuning of the resonance wavelength. As shown in Fig. 4(b), chip 1 and chip 2 are MCORs and are assembled into an independent $\theta/2\theta$ goniometer. The angle, θ, is the angle of incidence of chip 1, and φ is that of chip 2. Figures 4(c) and 4(d) present the optical-comb spectra for chip 1 and chip 2 when the angles of incidence are $\theta = 6.40^\circ$ and $\varphi = 14.86^\circ$, respectively. The selected modes have a Fano shape or are split due to the simultaneous coupling of TM_0 and TM_1 modes. The TM_0 and TM_1 modes generate degeneracy when the thickness of the guiding layer is increased beyond a certain finite value (defined as the degeneracy thickness).

By varying the angle of incidence, φ, of chip 2, while the angle of incidence, θ, of chip 1 remains fixed, single-mode spectra are obtained by using the mode-selection system based on the two directly coupled MCORs. When chip 2 is at angles of incidence of $\varphi_1 = 6.40^\circ$, $\varphi_2 = 10.04^\circ$, $\varphi_3 = 12.66^\circ$, and $\varphi_4 = 14.86^\circ$, the spectroscope detects single-mode peaks at $\lambda_1 = 1064.39$ nm, $\lambda_2 = 1067.62$ nm, $\lambda_3 = 1073.82$ nm, and $\lambda_4 = 1076.95$ nm, respectively. In addition, when the angle of incidence, φ, of chip 2 is fixed, the angle of incidence, θ, of chip 1 then changes according to the four points shown in the ATR peak. At $\theta = 6.40^\circ$, the incident light is fully coupled into chip 1, which results in the intensity of the output single-mode peak from chip 2 reaching a maximum. Additionally, when the light is incident without being coupled at point d, where $\theta = 6.90^\circ$, no single-mode peak output from chip 2 is found. When the light is incident at points b and c, where $\theta = 6.30^\circ$ and $\theta = 6.50^\circ$, respectively, part of the incident light is coupled into chip 1, and the intensity of the single mode is less than that at point a, as shown in Figs. 4(f) and 4(g).

IV. DISCUSSION

As shown in Eqs. (3) and (4), the linewidths of the single-mode peaks output from the mode-selection system based on the two directly coupled MCORs have a close relationship with the waveguide-layer thickness, h_1, in each MCOR. Therefore, if we wish to achieve a narrower linewidth for the single mode that is output from the system, the value of h_1 should be increased. In our experiments, MCORs with thicknesses of 0.1 and 0.26 mm are used to form the mode-selection system. Figures 5(a) and 5(b) show the optical-comb spectra for the MCORs with thicknesses of 0.10 and 0.26 mm, respectively; the free-space range (FSR), $\Delta\lambda$, and the linewidth of the mode, $\delta\lambda$, of the 0.26-mm MCOR are less than the corresponding values for the 0.10-mm MCOR, but the value of $\delta\lambda/\Delta\lambda$ for the 0.26-mm MCOR is greater than that for the 0.1-mm MCOR, as shown in Figs. 5(c) and 5(d). According to the numerical simulation, the addition to the MCOR thickness, h_1, results in an increase in the number of modes, m. Although the linewidth of each mode will be reduced in this case, the FSR is also reduced, and the value of $\delta\lambda/\Delta\lambda$ thus becomes closer to 1, which leads to the adjacent modes becoming increasingly difficult to distinguish because of the Rayleigh resolution limit. Therefore, in our experimental system, we use MCORs with thicknesses of 0.1 and 0.26 mm. Additionally, the single-mode peak is detected using the spectrograph from the system shown in Fig. 4(a). When the system consists of chips that both have a waveguide-layer thickness of 0.26 mm, we obtain a narrower linewidth for the single-mode peak, as shown in Fig. 5(e), where the linewidth of the single mode is 0.588 nm. When the angle of incidence, θ, of chip 1 is fixed, the output single-mode peak wavelength varies in tandem with the angle of incidence, φ, of chip 2. From experimental data, we find that the peak wavelengths are 1063.00, 1064.57, 1066.14, 1067.68, 1069.25, 1070.82, 1072.39, and 1073.96 nm when the angle of incidence, φ, of chip 2 is varied from φ_1 to φ_8, respectively.

However, under the same conditions, the MCOR with a thickness of 0.1 mm is used to replace chip 1 in the mode-selection system. This means that the mode-selection system used to obtain a single-mode peak now consists of MCORs with thicknesses of 0.26 and 0.1 mm. We detect a signal spectrum that does not have a single-mode output. Parts of the 0.1-mm MCOR mode and the 0.26-mm MCOR mode can be found as coherent resonances in the overlaps between the mode regions because the FSR $\Delta\lambda$ of the MCOR, with a thickness of 0.26 mm, is less than that for the MCOR with a thickness of 0.1 mm; this results in more than mode resonances occurring and not a single coherent mode output. Experimental data are shown in Fig. 5(f). Therefore, the mode-selection system must consist of MCORs of the same thickness, which can then provide a single-mode output.

V. CONCLUSION

Our demonstration of an optical-mode-selection system represents an important step toward integrated single-mode optical output. In addition to the consideration of the linewidths of the output modes and the tunable single modes in the discussion above, the power efficiency and loss of the device can also be improved through appropriate design and fabrication of the waveguide elements. Additionally, there are no fundamental limits on the linewidth and the wavelength of the single-mode output operation that can be obtained using the scheme presented here. Therefore, this simple, effective, and tunable optical system has huge potential for applications in optical communications and the optical-sensor field.

ACKNOWLEDGMENTS

Funding for this work is from the National Key Research and Development Program of China (Grants

No. 2017YFA0303701 and No. 2018YFA0306301), the National Natural Science Foundation of China (NSFC) (Grants No. 12104298, No. 11734011, No. 11764020, and No. 11974245), and the Shanghai Municipal Science and Technology Major Project (Grant No. 2019SHZDZX01-ZX06).

The authors declare that they have no conflict of interest.

[1] K. J. Vahala, Optical microcavities, Nature **106**, 839 (2003).
[2] K. E. Kreischer and R. J. Temkin, Single-Mode Operation of a High-Power, Step-Tunable Gyrotron, Phys. Rev. Lett. **59**, 547 (1987).
[3] L. R. Elias, G. Ramian, J. Hu, and A. Amir, Observation of Single-Mode Operation in a Free-Electron Laser, Phys. Rev. Lett. **57**, 424 (1986).
[4] D. K. Armani, T. J. Kippenberg, S. M. Spillane, and K. J. Vahala, Ultra-high-*Q* toroid microcavity on a chip, Nature **421**, 925 (2003).
[5] L. Feng, Z. J. Wong, R.-M. Ma, Y. Wang, and X. Zhang, Single-mode laser by parity–time symmetry breaking, Science **346**, 972 (2014).
[6] X. Yin and X. Zhang, Unidirectional light propagation at exceptional points, Nat. Mater. **12**, 175 (2013).
[7] Hossein Hodaei, Absar U. Hassan, Steffen Wittek, Hipolito Garcia-Gracia, Ramy El-Ganainy, Demetrios N. Christodoulides, and Mercedeh Khajavikhan, Enhanced sensitivity at higher-order exceptional points, Nature **548**, 187 (2017).
[8] Mikhail F. Limonov, Mikhail V. Rybin, Alexander N. Poddubny, and Yuri S. Kivshar, Fano resonances in photonics, Nat. Photonics **11**, 543 (2017).
[9] Ramy El-Ganainy, Konstantinos G. Makris, Mercedeh Khajavikhan, Ziad H. Musslimani, Stefan Rotter, and Demetrios N. Christodoulides, Non-Hermitian physics and *PT* symmetry, Nat. Phys. **14**, 11 (2018).
[10] H. Ghafouri-Shiraz, *Distributed Feedback Laser Diodes and Optical Tunable Filters* (Wiley, New York, 2003).
[11] Martin T. Hill, Yok-Siang Oei, Barry Smalbrugge, Youcai Zhu, Tjibbe de Vries, Peter J. van Veldhoven, Frank W. M. van Otten, Tom J. Eijkemans, Jarosław P. Turkiewicz, Huug de Waardt, *et al.*, Lasing in metallic-coated nanocavities, Nat. Photonics **1**, 589 (2007).
[12] Ren-Min Ma, Rupert F. Oulton, Volker J. Sorger, Guy Bartal, and Xiang Zhang, Room-temperature sub-diffraction-limited plasmon laser by total internal reflection, Nat. Mater. **10**, 110 (2011).
[13] S. F. Liew, B. Redding, L. Ge, G. S. Solomon, and H. Cao, Active control of emission directionality of semiconductor microdisk lasers, Appl. Phys. Lett. **104**, 231108 (2014).
[14] Liang Feng, Maurice Ayache, Yelong Jingqing Huang, Minghui Xu, Yanfeng Chen Lu, Yeshaiahu Fainman, and Axel Scherer, Nonreciprocal light propagation in a silicon photonic circuit, Science **333**, 729 (2011).
[15] A. Guo, G. Salamo, D. Duchesne, R. Morandotti, M. Volatier-Ravat, V. Aimez, G. Siviloglou, and D. Christodoulides, Observation of *PT*-Symmetry Breaking in Complex Optical Potentials, Phys. Rev. Lett. **103**, 093902 (2009).
[16] Christian E. Rüter, Konstantinos G. Makris, Ramy El-Ganainy, Demetrios N. Christodoulides, Mordechai Segev, and Detlef Kip, Observation of parity–time symmetry in optics, Nat. Phys. **6**, 192 (2010).
[17] Liang Feng, Ye-Long Xu, William S. Fegadolli, Ming-Hui Lu, José E. B. Oliveira, Vilson R. Almeida, Yan-Feng Chen, and Axel Scherer, Experimental demonstration of a unidirectional reflectionless parity–time metamaterial at optical frequencies, Nat. Mater. **12**, 108 (2012).
[18] Alois Regensburger, Christoph Bersch, Mohammad-Ali Miri, Georgy Onishchukov, Demetrios N. Christodoulides, and Ulf Peschel, Parity–time synthetic photonic lattices, Nature **488**, 167 (2012).
[19] L. He, S. K. Ozdemir, and L. Yang, Whispering gallery microcavity lasers, Laser Photonics Rev. **7**, 60 (2013).
[20] L. He, S. K. Ozdemir, J. Zhu, W. Kim, and L. Yang, Detecting single viruses and nanoparticles using whispering gallery microlasers, Nat. Nanotechnol. **6**, 428 (2011).
[21] Bo Peng, Şahin Kaya Özdemir, Fuchuan Lei, Faraz Monifi, Mariagiovanna Gianfreda, Gui Lu Long, Shanhui Fan, Franco Nori, Carl M. Bender, and Lan Yang, Parity–time-symmetric whispering-gallery microcavities, Nat. Phys. **10**, 394 (2014).
[22] H. L. Dai, L. Q. Yuan, C. Yin, Z. Q. Cao, and X. F. Chen, Direct Visualizing the Spin Hall Effect of Light via Ultrahigh-Order Modes, Phys. Rev. Lett. **124**, 053902 (2020).
[23] Y. Trabelsi, W. Belhadj, N. Ben Ali, and A. H. Aly, Theoretical study of tunable optical resonators in periodic and quasiperiodic one-dimensional photonic structures incorporating a nematic liquid crystal, Photonics **8**, 15 (2021).
[24] Q. H. Wei, H. L. Dai, H. R. Shan, H. G. Li, Z. Q. Cao, and X. F. Chen, All-photonic synapse based on iron-doped lithium niobate double metal-cladding waveguides, Phys. Rev. B **104**, 235308 (2021).
[25] H. G. Li, Z. Q. Cao, H. F. Lu, and Q. S. Shen, Free-space coupling of a light beam into a symmetrical metal-cladding optical waveguide, Appl. Phys. Lett. **83**, 2757 (2003).
[26] H. L. Dai, C. Yin, Z. Y. Xiao, Z. Q. Cao, and X. F. Chen, White Beam Lasing from a Hybrid Microcavity with Slab-Capillary Mode Coupling, Phys. Rev. Appl. **11**, 064055 (2019).
[27] H. R. Shan, Q. H. Wei, H. L. Dai, and X. F. Chen, Sensitive detection of orthogonal polarization intensity ratio via metal-cladding waveguide, Opt. Lasers Eng. **151**, 106920 (2022).
[28] H. L. Dai, C. Yin, X. N. Ye, B. Jiang, M. W. Ran, Z. Q. Cao, and X. F. Chen, A possible pathogenetic factor of sickle-cell disease based on fluorescent analysis via an optofluidic resonator, Sci. Rep. **7**, 3174 (2017).
[29] Y. Wang, Z. Q. Cao, T. Y. Yu, H. G. Li, and Q. S. Shen, Enhancement of the superprism effect based on the strong dispersion effect of ultrahigh-order modes, Opt. Lett. **33**, 1276 (2008).
[30] I. P. Kaminow, W. L. Mammer, and H. P. Weber, Metal-clad optical waveguides: Analytical and experimental study, Appl. Opt. **13**, 396 (1974).
[31] See the Supplemental Material at http://link.aps.org/supplemental/10.1103/PhysRevApplied.19.034046 for the

dispersion properties, ultrahigh-order modes, the discrete ATR dips of the ultrahigh-order modes, the tunable comb filter, and the wavelength variation relationship with the incident angle of light; it also includes Refs. [30,34].

[32] H. L. Dai, B. Jiang, C. Yin, Z. Q. Cao, and X. F. Chen, Ultralow-threshold continuous-wave lasing assisted by a metallic optofluidic cavity exploiting continuous pump, Opt. Lett. **43**, 847 (2018).

[33] L. Chen, Z. Q. Cao, F. Ou, H. G. Li, Q. S. Shen, and H. C. Qiao, Observation of large positive and negative lateral shifts of a reflected beam from symmetrical metal-cladding waveguides, Opt. Lett. **32**, 1432 (2007).

[34] H. F. Lu, Z. Q. Cao, H. G. Li, and Q. S. Shen, Study of ultrahigh-order modes in a symmetrical metal-cladding optical waveguide, Appl. Phys. Lett. **85**, 4579 (2004).